Photo-oxidation of Acetone to Formic Acid in Synthetic Air and Its Atmospheric Implication

ARTICLE *in* THE JOURNAL OF PHYSICAL CHEMISTRY A · JUNE 2015

Impact Factor: 2.69 · DOI: 10.1021/acs.jpca.5b04905 · Source: PubMed

3 AUTHORS:

Aparajeo Chattopadhyay

Indian Association for the Cultivation of Science

2 PUBLICATIONS **4** CITATIONS

SEE PROFILE

Piyali Chatterjee

Indian Association for the Cultivation of Science

3 PUBLICATIONS **3** CITATIONS

SEE PROFILE

Tapas Chakraborty

Indian Association for the Cultivation of Science

107 PUBLICATIONS **853** CITATIONS

SEE PROFILE

THE JOURNAL OF PHYSICAL CHEMISTRY A

Article

pubs.acs.org/JPCA

Photo-oxidation of Acetone to Formic Acid in Synthetic Air and Its Atmospheric Implication

Aparajeo Chattopadhyay,* Piyali Chatterjee, and Tapas Chakraborty*

Department of Physical Chemistry, Indian Association for the Cultivation of Science, 2A Raja S. C. Mullick Road, Jadavpur, Kolkata 700032, India

Supporting Information

ABSTRACT: Acetone photo-oxidation in synthetic air under exposure of 311 nm ultraviolet light has been studied, and the photo-oxidation products are identified by means of infrared spectroscopy. Analysis reveals that formic acid is one of the major products, although there have been debates in the past concerning the authenticity of formation of this acid in synthetic air via the photo-oxidation pathway. The quantum yield of formation of this acid is similar to that of other major photoproducts like methanol, formaldehyde, and carbon monoxide. The reaction yield, however, decreases with an increase in total air pressure in the reaction cell, but it is still significant at pressures relevant to tropospheric conditions. A kinetic model has been used to simulate the measured reaction kinetics, and the quantum yields predicted by the model are found to be consistent with the measured yields for different durations of light exposure. The same model has also been used to investigate the effect of atmospheric nitric oxide on the fate of formation of this acid in the troposphere. Although nitric oxide is known to be a quencher of peroxy radicals, the precursors of formaldehyde and formic acid in acetone photo-oxidation, but our model predicts that this oxide plays a positive role in the overall reaction kinetics for production of this acid in the troposphere.

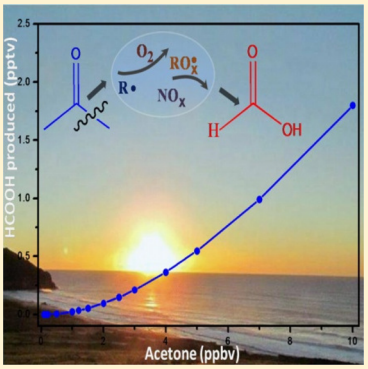

I. INTRODUCTION

Formic acid is an important component of the organic matters present in the atmosphere.[1−3] It is one of the largest sources of atmospheric acidity that controls the aqueous reactions in the clouds and aerosols, and it also contributes to the acidity of rainwater.[1,3] It influences the atmospheric composition by balancing the concentrations of atmospheric radicals that lead to ozone formation in the lower region of the atmosphere.[1,3] The annual atmospheric budget of formic acid is quite high, ∼100−120 Tg,[2] and a major fraction of this amount is produced by means of atmospheric oxidations of different volatile organic compounds emitted from bio- and anthropogenic sources. However, this abundance has been estimated to be several times larger compared to the known sources, and it has been suggested that one of the possible reasons for this discrepancy is the uncertainty in formation of this acid under tropospheric conditions via photochemical oxidation pathways.[2,3] Therefore, for reliable atmospheric modeling studies, authentic and quantitative data for formic acid production via photo-oxidation pathways of different VOCs of high atmospheric abundance are essential.[3−5]

In this paper, we report an unambiguous observation of formic acid production by photo-oxidation of acetone in synthetic air under exposure of a UV wavelength that is abundant in the lower troposphere. From the atmospheric perspective, acetone is a partially oxygenated hydrocarbon of nonmethane origin. Photochemistry of acetone in the atmosphere has been suggested to be important as a significant contributor to atmospheric $HO_x^•$ radicals that play a very important role in tropospheric oxidation and removal of a large variety of other anthropogenic pollutants.[6] Formic acid production via photo-oxidation of acetone is one of the controversial topics in the rich history of laboratory studies of photochemistry of this molecule. Osborne et al. first reported production of formic acid in vapor phase photochemistry of acetone in the presence of oxygen.[7] Shortly afterward, Pearson refuted this claim, and in a long run of experiments employing the same experimental conditions the author could not detect formic acid in spite of using the same spectroscopic probing method.[8] In five decades since these two reports, many studies of acetone photo-oxidation have appeared in the literature,[9−16] but the reaction leading to formic acid was never discussed. In 1984, Gardner et al. stated that formic acid is an expected product of acetone photo-oxidation,[11] but since the authors used a gas chromatographic method for quantitative estimation of the photoproducts the acidic species, if produced at all, remained undetected. More recently, Ravishankara and coworkers investigated acetone photo-oxidation under simulated tropospheric conditions, and the primary aim of the studies was to measure the quantum yield of acetone photolysis as a function of pressure and wavelength of the photolysis light.[13]

Here, in addition to demonstrating the photo-oxidative formation of formic acid from acetone, a mechanism for formation pathway of this acid has also been suggested. The

Received: May 22, 2015
Revised: June 17, 2015

DOI: 10.1021/acs.jpca.5b04905
J. Phys. Chem. A XXXX, XXX, XXX−XXX

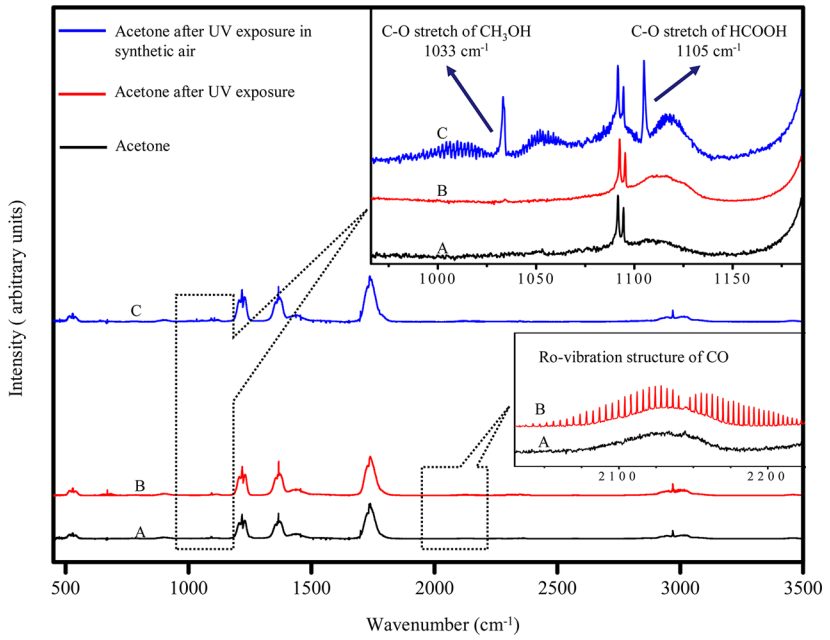

Figure 1. FTIR spectra of acetone vapor at 30 °C diluted in N_2 at a total pressure of 300 mbar (A) following photolysis (UV wavelength 311 nm) of the same in the absence of air for 180 min (B) and photolyzed (in the synthetic air) gas mixture for the same duration of light exposure (C). The inset of trace B shows the ro-vibrational features of the stretching fundamental of carbon monoxide. The inset on trace-C shows ro-vibrational structures of methanol and formic acid produced for light irradiation in synthetic air.

validity of the mechanism is corroborated invoking a kinetic model that can satisfactorily reproduce the quantum yield of production of the acid under the experimental conditions employed. In this paper, the results have been presented in the following organization. First, an IR spectral signature for authentic formation of the acid by acetone photo-oxidation is presented. The quantum yield of the acid produced along with other photoproducts and how the yields vary with reaction parameters, are then discussed. A possible pathway for formic acid production is discussed, and a model has been performed involving the kinetics of more than 40 chemical steps suggested in the mechanism. Finally, concerning tropospheric significance of this photo-oxidation study, we discuss the impact of atmospheric nitric oxide on yields of formic acid production and also discuss the expected production of the acid via this channel in the troposphere.

II. EXPERIMENTAL METHODS

Photo-oxidation of acetone vapor was carried out in a cylindrical quartz cell of length 18 cm and inner diameter 3 cm. Two polished optical-grade flat KBr windows were fitted at the two open ends of the cell, and the joints were vacuum sealed using silicon rubber o-rings. For identification of the reaction products and also to monitor the progress of the reaction at definite time intervals after switching the UV lamps on, a commercial FTIR spectrometer (IFS 66S, Bruker Optics) was employed. The cell body has three other ports to attach the following: (i) a small turbomolecular vacuum pump (Pfeiffer Vacuum) backed by a dry diaphragm pump for evacuation of the cell, (ii) a high-pressure capacitive diaphragm gauge (CMR 361, Pfeiffer Vacuum) to monitor pressures, and (iii) a glass sample reservoir. The sample introduction into the cell from the reservoir was controlled using a Swagelok precision metering valve. A homemade temperature sensor of accuracy ±1 °C was used for recording the cell temperature throughout the experiment. The reaction cell was placed directly into the sample compartment of the FTIR spectrometer, and three similar UV−B lamps of emission maximum at 311 nm (Philips TL 01, 20 W) were installed around the reaction cell as light sources to carry out the photolysis. The instrument resolution of the FTIR spectrometer used to record spectra was 0.25 cm^{-1}. From time to time, we also used a second FTIR spectrometer, Tensor 27 (Bruker Optics), and the instrument was operated at a spectral resolution of 0.5 cm^{-1}. The software for spectral data acquisition, OPUS version 7.0, was provided by the manufacturer of the spectrometer (Bruker Optics), and the same software was used for the purpose of displaying the recorded spectra. Each measurement was repeated at least three times to check the reproducibility of the results. Proper arrangement of air flow around the cell was made to keep the cell temperature at 30 °C.

Spectroscopic-grade acetone was obtained from Spectrochem India Pvt Ltd. Before use, the procured compound was degassed by means of several freeze−pump−thaw cycles. The purity of nitrogen and oxygen gases used was ∼99.99%. NO was prepared before use by reaction between $NaNO_2$ and $FeSO_4{\cdot}7H_2O$.[17]

III. RESULTS AND DISCUSSION

A. IR Spectral Identification of Formic Acid. Photo-oxidation of acetone was performed while maintaining the following reaction conditions. Acetone vapor was diluted in synthetic air (N_2:O_2 = 4:1) in the reactor cell, and the total pressure of the gas mixture during UV (311 nm) irradiation was 300 mbar. The progress of the photochemical reaction was monitored by recording FTIR spectra at a regular interval of time. A comparison of the fingerprint segments of the three such spectra recorded in the presence and in the absence of synthetic air in the reaction cell is shown in Figure 1. The lowermost panel depicts the IR spectrum recorded before UV irradiation and the middle panel for irradiation of the vapor for 180 min in the absence of synthetic air. In later conditions, the

DOI: 10.1021/acs.jpca.5b04905
J. Phys. Chem. A XXXX, XXX, XXX−XXX

most prominent signature of the reaction is the appearance of typical rovibrational features of carbon monoxide with band center ~2150 cm^{-1}. For reaction in synthetic air, two new bands show up around 1100 cm^{-1} (top panel). The associated rotational fine structures are shown in the inset in a blown-up scale. The band centered at 1105 cm^{-1} is identified as the C−O stretching fundamental of formic acid, and the other one at 1033 cm^{-1} is identified as the C−O stretching fundamental of methanol. These transitions with the characteristic P, Q, and R branches are the unambiguous signatures for production of formic acid along with methanol.

In most of the previous studies, formaldehyde was identified as the key photo-oxidation product, and the reaction parameters were assigned with respect to this species.[8−11,13] However, the $\nu_{C=O}$ band of formaldehyde in the infrared spectrum appears to be overlapped with that of acetone. Therefore, the kinetics and quantum yield for formation of this product have been estimated by monitoring the aldehydic C−H stretching fundamental of the molecule at 2778 cm^{-1}. From the IR spectral data, carbon dioxide (CO_2) is also identified as a photo-oxidation product, but quantitative estimation of this species was not attempted because of interference of the atmospheric CO_2.

B. Estimation of Kinetic Parameters. For the above-mentioned reaction scheme, accumulation of four major photoproducts, HCOOH, CH_3OH, HCHO, and CO, with increasing duration of light irradiation in the reactor cell is shown in Figure 2.

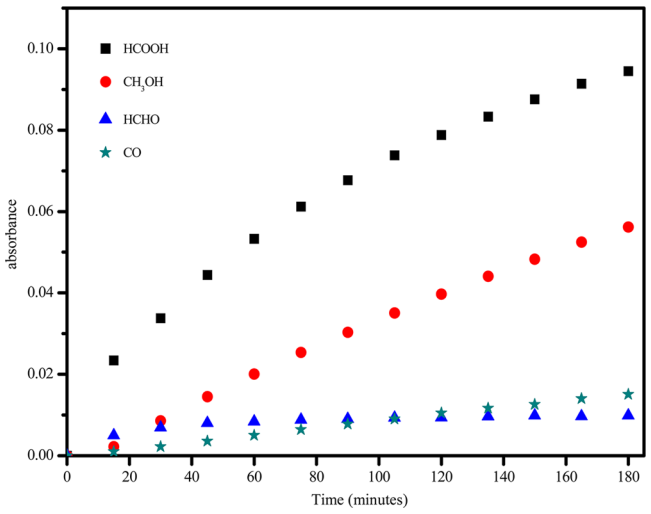

Figure 2. Accumulation of major photo-oxidation products (CO, HCHO, CH_3OH, and HCOOH) in the reaction cell indicated in terms of change in absorbance of the species with time following switching on the UV light.

The changes are depicted in terms of increase in absorbance of a key characteristic band for each of the products (Table 1). A time-dependent increase in concentration has been estimated using absorption cross-section data, which have been taken from the PNNL database.[18]

The plots displayed in Figure 2 indicate that, except formic acid, the concentration of other photoproducts increases almost linearly with time. For formic acid, the primary reason for deviation from the linear behavior is due to large tendency of this acid vapor to get adsorbed on the inner cell walls of the quartz reactor. To monitor the kinetics of this adsorption process, we performed the following two additional measurements. First, after 3 h of continuous UV irradiation, the lamps were switched off and the decrease of the accumulated concentrations of different species within the cell volume was monitored at a regular interval of time, and such changes for HCOOH and CH_3OH are shown in Figure 3a. Clearly, the loss of HCOOH occurs at a much faster rate compared to that of CH_3OH. To eliminate the possibility that this change is not due to reaction of the acid with any of the other gaseous species present in the reactor, the time-dependent change in concentration of the pure vapor of formic acid introduced into the cell was also measured as depicted in Figure 3b. For the latter purpose, pure formic acid vapor was diluted into 300 mbar of synthetic air in the reactor cell, and the decrease of its concentration within the cell volume due to adsorption loss was measured.

A comparison of the two plots indicates that the IR signals in both cases decrease exponentially; i.e., the loss rate of HCOOH in both situations is similar. Thus, for kinetic treatments of photochemical formation of this acid we assume that its accumulation with time within the reactor cell, similar to other photoproducts, occurs linearly. Therefore, to work out the effective reaction rate from the depicted IR spectroscopy data, the following two gross steps associated with the reaction have been considered where k_1 is the photochemical formation rate constant of HCOOH and k_2 is the adsorption loss rate constant.

$$CH_3COCH_3 + O_2 \xrightarrow{k_1} HCOOH \xrightarrow{k_2} HCOOH_{unadsorbed}$$

The effective rate of formation of HCOOH, which is actually probed as an IR absorption signal, could be expressed as

$$d[HCOOH]/dt = k_1 - k_2[HCOOH] \quad (1)$$

The solution of this equation can be expressed as

$$[HCOOH]_t = (k_1/k_2)[1 - \exp(-k_2 t)] \quad (2)$$

Here, $[HCOOH]_t$ is the measured concentration of HCOOH at time t after switching on the photolysis lamps. The first-order adsorption rate constant, k_2, is estimated from the kinetics data presented in Figure 3b.

Using these data, we estimate from eq 2 the value for k_1, which in turn provides the actual concentration of HCOOH produced at time t

$$[HCOOH]_{actual} = k_1 t$$

Table 1. Different Infrared Fundamentals Used to Identify the Major Photoproducts[a]

species	HCOOH	CH_3OH	HCHO	CO	CH_3COCH_3
frequency (cm^{-1}) (obsd)	1105	1033	2778	2173	2970
vibration mode (fundamental)	$C-O_{stretch}$	$C-O_{stretch}$	$C-H_{stretch}$	$C-O_{stretch}$	$C-H_{stretch}$
absorption cross-section (cm^2/ molecule)	1.3×10^{-18}	4.4×10^{-19}	4.3×10^{-19}	8.8×10^{-19}	5.6×10^{-20}

[a]The corresponding frequencies and absorption cross-section values are also shown.

DOI: 10.1021/acs.jpca.5b04905
J. Phys. Chem. A XXXX, XXX, XXX−XXX

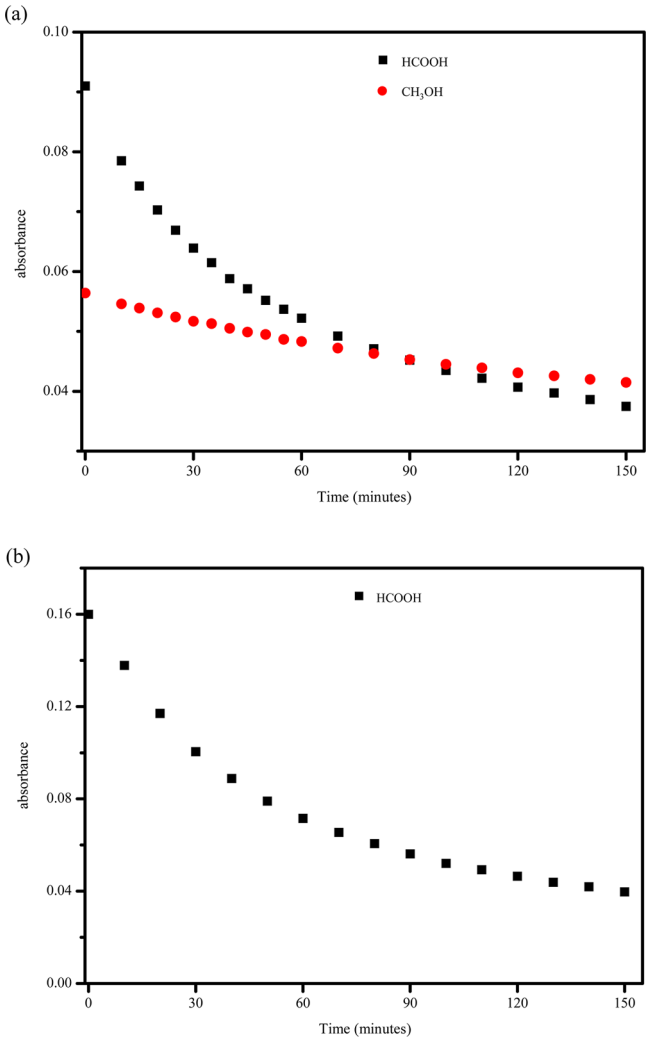

Figure 3. Time-dependent decrease of accumulated formic acid and methanol in the reaction cell following switching the UV lamp off after 3 h of light irradiation (a) and the loss rate of pure formic acid vapor in the same cell (b).

C. Quantum Yields of the Photoproducts. For estimation of the quantum yields of the photoproducts, it is necessary to measure the intensity of the photolysis light used under the experimental conditions. For this purpose, we proceeded in the following way. First, acetone itself was used as an actinometric substance. The quantum yield for CO production by UV photolysis at a wavelength similar to that reported by Herr et al. was used as the reference data.[19] The reaction conditions employed in our measurement, i.e., with respect to sample vapor pressure, cell temperature, excitation wavelength, etc., were same as those used in ref 19. The effective intensity of the light estimated by fitting CO production quantum yield is shown in Table 4. Finally, to estimate the quantum yield of formic acid production using the light intensity data, the adsorption corrected concentrations obtained by the method as described above were used.

The plots depicted in Figure 4 indicate that the quantum yields (QY) of all four major products vary with the time of light irradiation. During the first 60 min of irradiation, the QY of CO appears to remain unchanged, but those of CH_3OH, HCHO, and HCOOH decrease slowly. Initially, the QY of HCHO appears larger compared to that of HCOOH, but the

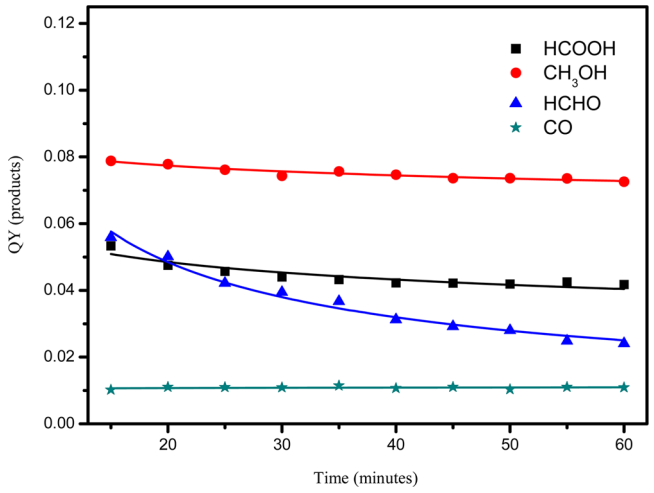

Figure 4. Variation of quantum yields (QY) of the major photoproducts with increasing irradiation time.

situation is reversed afterward. Such temporal behavior implies that formic acid formation occurs in multiple stages and the product methanol may undergo further oxidation to produce formic acid.

D. Reaction Modeling. The temporal behavior depicted in Figure 4 implies that many primary and secondary reactions are involved in formic acid production in acetone photo-oxidation, and a list of reactions which could be involved in the whole process is shown in Table 2 along with their rate parameters. A reaction modeling has been performed using the depicted kinetic data, the computer program Acuchem, developed by Braun et al.,[20] has been used for this purpose, and the literature shows that many other groups have also used this code.[21−24] The code solves a set of differential equations corresponding to rate laws of interrelated chemical reactions, and thus, it become useful to depict the temporal behavior of complex reactions. The heart of the program is the DDRIV3 integrator. For input, the program requires the list of the reactions involved along with their rate constants, reaction orders, concentrations of reactants, and reaction time. As output, one gets the temporal profile with respect to different reactants and products.

Occurrence of an α-cleavage (Norrish Type I reaction) following absorption of a UV photon (311 nm) that results formation of a methyl and an acetyl radical is the reaction initiation step. Both radicals have a strong affinity for oxygen and thus generate peroxymethyl and peroxyacetyl radicals, which are the precursors of methanol and formaldehyde. Under continuous exposure, formaldehyde is likely to undergo further dissociation via two different reaction channels whose quantum yields are known and eventually leads to formic acid production. Methanol does not absorb this wavelength, but it can be further oxidized by $HO_x^{\bullet}$ radicals, which can be generated under the reaction conditions used as depicted in Table 2.

The quantum yields of three products obtained from our modeling study are presented in Table 3. A comparison of these data with those of experimental data for atmospheric pressure is also given. It is apparent that the agreements are satisfactory. The data reported by Gardner et al. are also presented for comparison with our results.[11] In Table 4, the experimental conditions used in the present and previous study of Gardner et al. are presented. Furthermore, to verify whether the estimated quantum yield is the result of a pure gas-phase

DOI: 10.1021/acs.jpca.5b04905
J. Phys. Chem. A XXXX, XXX, XXX−XXX

Table 2. Set of Reactions Used in Modeling Acetone Photo-oxidation

no.	reaction[a]	rate constant[b]	ref
1	$CH_3COCH_3 \rightarrow CH_3 + CH_3CO$	QY = 0.0771	11
2	$CH_3 + O_2 + M \rightarrow CH_3O_2 + M$	$K_0 = 4.5 \times 10^{-31}$	25
		$K_\infty = 1.8 \times 10^{-12}$	
3	$CH_3CO + O_2 + M \rightarrow CH_3COO_2 + M$	3.64×10^{-12}	26
4a	$2\ CH_3O_2 \rightarrow CH_3OH + HCHO + O_2$	2.80×10^{-13}	25
4b	$\rightarrow 2\ CH_3O + O_2$	1.40×10^{-13}	
5	$CH_3O + O_2 \rightarrow HCHO + HO_2$	1.90×10^{-15}	25
6	$CH_2OH + O_2 \rightarrow HCHO + HO_2$	9.70×10^{-12}	27
7	$CH_3O + CH_3O \rightarrow HCHO + CH_3OH$	3.00×10^{-11}	28
8	$CH_3O + HO_2 \rightarrow CH_3OH + O_2$	3.00×10^{-11}	29
9	$CH_3COO_2 + CH_3COO_2 \rightarrow CH_3CO_2 + CH_3CO_2 + O_2$	1.60×10^{-11}	30
10a	$CH_3O_2 + CH_3COO_2 \rightarrow CH_3O + CH_3CO_2 + O_2$	9.00×10^{-12}	31
10b	$\rightarrow CH_3COOH + HCHO + O_2$	1.00×10^{-12}	
11	$CH_3CO_2 \rightarrow CH_3 + CO_2$	1.00×10^{06}	13
12	$HO_2 + HO_2 \rightarrow H_2O_2 + O_2$	1.18×10^{-12}	25
13a	$HO_2 + CH_3COO_2 \rightarrow CH_3COO_2H + O_2$	1.00×10^{-11}	29
13b	$\rightarrow CH_3CO_2H + O_3$	4.00×10^{-12}	
14a	$HCHO \rightarrow H + HCO$	QY = 0.68	27[c]
14b	$\rightarrow H_2 + CO$	QY = 0.32	
15	$H + O_2 \rightarrow HO_2$	1.30×10^{-12}	25
16	$HCO + O_2 \rightarrow HO_2 + CO$	5.60×10^{-12}	25
17	$HO_2 + HCHO \rightarrow O_2CH_2OH$	5.00×10^{-14}	25
18	$O_2CH_2OH \rightarrow HO_2 + HCHO$	150.7	32
19	$O_2CH_2OH + HO_2 \rightarrow HCOOH + H_2O + O_2$	1.26×10^{-11}	32
20a	$O_2CH_2OH + O_2CH_2OH \rightarrow HOCH_2O + HOCH_2O + O_2$	5.50×10^{-12}	32
20b	$\rightarrow HCOOH + CH_2OHOH + O_2$	7.07×10^{-13}	
21	$O_2 + HOCH_2O \rightarrow HCOOH + HO_2$	3.50×10^{-14}	33
22	$CH_3CO + O_2 \rightarrow OH + products$	9.00×10^{-14}	26
23	$OH + HCHO \rightarrow H_2O + HCO$	9.20×10^{-12}	25
24a	$OH + CH_3OH \rightarrow H_2O + CH_2OH$	7.65×10^{-13}	27
24b	$\rightarrow H_2O + CH_3O$	1.35×10^{-13}	
25	$OH + HCOOH \rightarrow products$	4.50×10^{-13}	27
26	$OH + HCHO \rightarrow HCOOH + H$	2.01×10^{-13}	34
27	$H_2O_2 \rightarrow 2\ OH$	2.82×10^{-06}	35
28	$CO + OH \rightarrow CO_2 + H$	2.40×10^{-13}	25
29a	$HO_2 + CH_3O_2 \rightarrow CH_3O_2H + O_2$	1.20×10^{-12}	36
29b	$\rightarrow HCHO + O_2 + H_2O$	1.04×10^{-13}	37
30a	$OH + CH_3O_2H \rightarrow CH_3O_2 + H_2O$	5.18×10^{-12}	38
30b	$\rightarrow CH_2O_2H + H_2O$	1.82×10^{-12}	39
31	$OH + HO_2 \rightarrow H_2O + O_2$	1.10×10^{-10}	39
32	$OH + H_2O_2 \rightarrow HO_2 + H_2O$	1.70×10^{-12}	39
33a	$H + HO_2 \rightarrow H_2 + O_2$	5.60×10^{-12}	32
33b	$\rightarrow OH + OH$	7.20×10^{-11}	
33c	$\rightarrow H_2O + O$	2.40×10^{-12}	
34	$O + H_2O_2 \rightarrow OH + HO_2$	1.70×10^{-15}	32
35	$OH + H_2 \rightarrow H_2O + H$	6.70×10^{-15}	32
36a	$OH + OH \rightarrow H_2O + O$	1.48×10^{-12}	32
36b	$OH + OH + M \rightarrow H_2O_2 + M$	6.20×10^{-12}	32
37	$OH + O_3 \rightarrow HO_2 + O_2$	7.30×10^{-14}	25
38	$HO_2 + O_3 \rightarrow OH + 2O_2$	2.00×10^{-15}	25
39	$HCO + HCO \rightarrow HCHO + CO$	7.50×10^{-11}	40
40	$HCOOH \rightarrow$ adsorbed	1.40×10^{-04}	[d]

[a]M = inert gases used, He, N_2, Ar, O_2, etc. [b]Units of the rate constants used: first order, s^{-1}; second order, $cm^3\ molecule^{-1}\ s^{-1}$; for termolecular reactions the equivalent second-order rate constants has been used. [c]Photochemical dissociation rate of HCHO was estimated in the present study. [d]Estimated in the present study.

reaction or contributions from surface-catalyzed reactions, we have measured quantum yields in two different reaction cells that have different surface/volume ratios. However, no notable change was observed (results are given in the Supporting Information). Thus, we infer that the quantum yield data given in Table 3 are entirely due to gas-phase reactions.

E. Quantum Yields and Gas-Pressure of the Reactor. The effect of higher oxygen pressure on quantum yields of

DOI: 10.1021/acs.jpca.5b04905
J. Phys. Chem. A XXXX, XXX, XXX−XXX

Table 3. Quantum Yields of Different Photoproducts Obtained from Experiment and Simulation in Present Study[a]

	result of present study		result of Gardner et al.[11]	
species	expt	simulation	expt	simulation
HCOOH	0.0075	0.0054		0.035
CH_3OH	0.0255	0.0157	0.019	0.026
HCHO	0.0160	0.0179	0.025	0.022

[a]The quantum yields reported for methanol and formaldehyde in ref 11 are also given in the table for a comparison.

several oxygenated species are shown in Figure 5. To perform this study, partial pressure of acetone in the reactor was kept fixed (~10 mbar) while that of O_2 was varied. Dry excess nitrogen was added to maintain the total pressure of 100 mbar in each experimental run. It is seen that excess oxygen has distinct effects on the yields of formic acid and methanol. The yield of formic acid is increased, but that of methanol is reduced, and we suggest that the secondary reactions of methanol particularly with OH radical produced in step 22 (Table 2) could be responsible for this change. The same trend has also been obtained from simulation study (shown below in Figure 6). The quantum yield of formaldehyde also shows a small increase, but this happens to a much lesser extent compared to that of formic acid.

In Figure 6, the pressure-dependent (O_2) changes of relative quantum yields of different products as obtained from the modeling study are presented. Good agreement between Figures 5 and 6 corroborates the reaction mechanism depicted in Table 2. The agreement between modeling and measured behavior also indicates the importance of secondary reactions in the formation and removal of intermediate compounds, e.g., methanol. The species particularly important for these secondary reactions could be OH radicals.

The observed effects of total pressure on quantum yields of different products are shown in Table 5. In all of the experimental runs, acetone concentration was kept fixed, and the pressure of synthetic air (1:4 ratio of oxygen to nitrogen) was increased. It is seen that with increasing pressure within the reactor quantum yields of all the products are decreased. A straightforward interpretation of the observation is due to positive volume of activation of the photodissociation reactions involved, but the other possibility is collisional de-energization of the radical intermediates produced at higher pressures.

F. Atmospheric Implication of Acetone Photo-oxidation: Effects of NO. We acknowledge that the experimental finding of formic acid production in the photo-oxidation of acetone performed in a laboratory reaction cell and the associated reaction modeling as presented above might not be a guarantee that these could be significant, in a quantitative perspective, to what actually happens in the troposphere. A significant source of discrepancy is the reactions of the intermediates shown in Table 2 with many active species present in the atmosphere, and a key reaction in this respect is

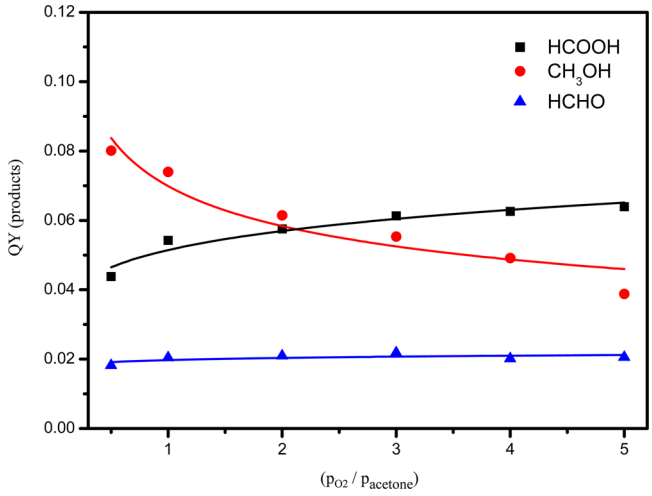

Figure 5. Effects of increasing oxygen partial pressure on QYs of different photoproducts. The partial pressure of acetone (10 mbar) and total pressure (100 mbar) of the reaction cell were kept same for each experimental run.

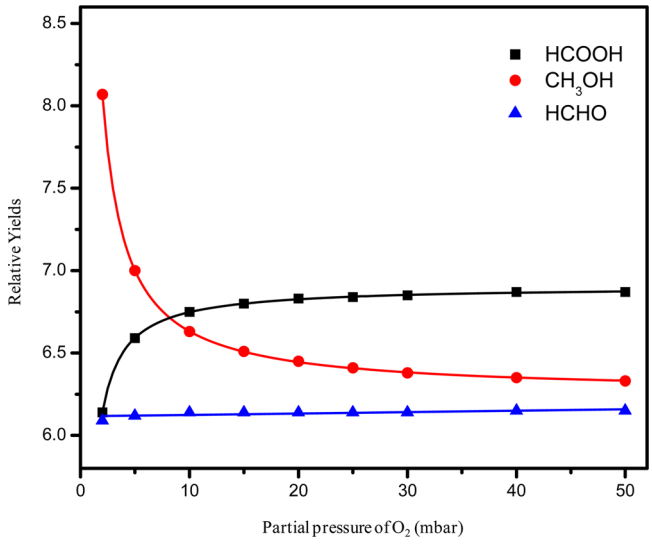

Figure 6. Variation of relative yields of different photoproducts with increasing partial pressure of O_2 obtained from modeling studies.

Table 5. Variation of Quantum Yields of Different Photoproducts with Increasing Total Pressure in the Reaction Cell

total pressure (mbar)	acetone conc (molecules·cm^{-3})	QY_{HCOOH}	QY_{CH_3OH}	QY_{HCHO}
100	1.69×10^{17}	0.056	0.105	0.046
200	1.66×10^{17}	0.052	0.089	0.044
650	1.78×10^{17}	0.039	0.047	0.035
940	1.83×10^{17}	0.031	0.038	0.029

Table 4. Details of Reaction Conditions Used in Present Study and Study of Gardner et al.[11]

reaction conditions	acetone pressure (mbar)	total pressure (atm)	T (°C)	exposure time (min)	wavelength of light (nm)	intensity of light (quanta cm^{-3} s^{-1})
present study	~0.5	1	30	180	311	1×10^{12}
Gardner et al.[11]	~0.5	1	25.5	240−1455	313	$0.86-1.12 \times 10^{11}$

DOI: 10.1021/acs.jpca.5b04905
J. Phys. Chem. A XXXX, XXX, XXX−XXX

between peroxy radicals and nitric oxide. The rate constants for reactions of nitric oxide with the following four peroxy radicals, HO_2, CH_3O_2, CH_3COO_2, and $HOCH_2O_2$, as available in the literature, are presented in Table 6.

Table 6. Rate Constants of the Reactions of NO with Peroxy Radicals

no.	reaction	rate constant[27] (cm^3 $molecule^{-1}$ s^{-1})
41	$NO + HO_2 \rightarrow HO + NO_2$	8.5×10^{-12}
42	$NO + CH_3O_2 \rightarrow CH_3O + NO_2$	7.7×10^{-12}
	$NO + CH_3O_2 + M \rightarrow CH_3ONO_2 + M$	
43	$NO + CH_3COO_2 \rightarrow CH_3CO_2 + NO_2$	2.0×10^{-11}
44	$NO + HOCH_2O_2 \rightarrow HOCH_2O + NO_2$	5.6×10^{-12}

In the cell photo-oxidation reactions, we have attempted to see also how the production of HCOOH and other products are affected by nitric oxide. To do this, we kept in mind the relative abundances of acetone and nitrogen oxides in the atmopshere, which are about 1 ppbv for acetone,[6] and 10−50 pptv of different NO_x.[41] Thus, in our reaction cell the concentrations of NO were taken about 0.03−0.04 times smaller compared to that of acetone, and the results are shown in Table 7. A mid-IR band near 1875 cm^{-1}, which has a cross section of 2.8×10^{-19} cm^2/molecule,[18] has been used to monitor its concentration changes.

It is somewhat surprising from the reaction data presented in Table 7 that yields of all three oxygenated products, HCOOH, HCHO, and CH_3OH, remain somewhat insensitive to the presence of NO. For further corroboration of these measured data, modeling studies were performed incorporating the reactions listed in Table 6, and the results are presented in Figure 7. It is seen that the modeling results are consistent with experimental data that the quantum yields of different photoproducts are not affected noticeably in the presence of NO.

The other important reason for acetone photo-oxidation parameters being different in the earth's atmosphere compared to what have been observed here in a cell study is the vastness of the former, where the concentrations of the reactants are much smaller compared to those used for laboratory study and where acetone undergoes photodissociation at a much slower rate. To get an idea about how formic acid production yield could be different in such situations, we have performed reaction modeling considering actual atmospheric abundance of acetone and its atmospheric photodissociation lifetime. The former is about 1 ppbv, and the atmospheric photodissociation rate constant of acetone, $k \approx 5 \times 10^{-7}$ s^{-1}. The reactions used to perform modeling under this condition are listed in Table 8.

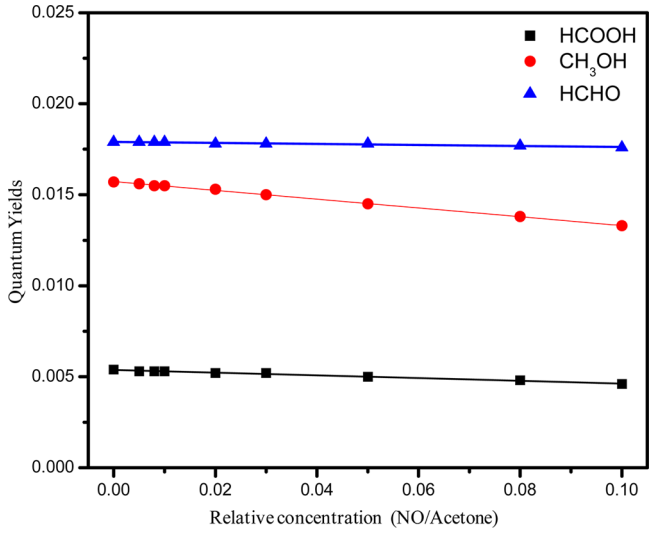

Figure 7. Effect of NO concentration on quantum yields of different photoproducts obtained from modeling studies.

The natural abundances of other atmospheric species considered in modeling are given in Table 9.

Table 8. Reactions Used in Atmospheric Modeling

reaction	rate constant	ref
$CH_3COCH_3 \rightarrow CH_3 + CH_3CO$	1×10^{-7} to 1×10^{-6} s^{-1}	13
reactions 2−13b as listed in Table 2		
$HCHO \rightarrow H + HCO$	1.109×10^{-5} s^{-1}	35
$\rightarrow H_2 + CO$	2.033×10^{-5} s^{-1}	
reactions 15−39 as listed in Table 2		
reactions 41−44 as listed in Table 6		

Table 9. Chemicals and Their Atmospheric Abundances Used in Atmospheric Modeling

species	concn	ref
acetone	0.2−3 ppbv	6
NO	10−50 pptv	41
OH	0.045 pptv	41
O_3	40 ppbv	41

The effect of NO on HCOOH production yield under such conditions is shown in Figure 8a. To perform this simulation, the concentration of acetone and atmospheric photodissociation rate constant of acetone are considered 1 ppbv and $k \approx 5 \times 10^{-7}$ s^{-1}, respectively. Here, the prediction is in contrast to normal expectations; i.e., the yield of HCOOH production increases significantly with an increase in NO concentration,

Table 7. Effect of NO on Yields of the Photoproducts[a]

set	$n_{NO}/n_{acetone}$	$n_{acetone}$	n_{NO}	n_{HCOOH}	n_{HCHO}	n_{CH_3OH}
1		8.83×10^{16}		3.12×10^{14}	4.39×10^{14}	3.18×10^{14}
	0.033	9.70×10^{16}	3.19×10^{15}	2.90×10^{14}	3.36×10^{14}	2.29×10^{14}
2		7.65×10^{16}		3.56×10^{14}	4.52×10^{14}	1.52×10^{14}
	0.036	7.22×10^{16}	2.61×10^{15}	3.56×10^{14}	5.43×10^{14}	2.02×10^{14}
3		1.02×10^{17}		3.90×10^{14}	4.91×10^{14}	2.02×10^{14}
	0.033	8.49×10^{16}	2.82×10^{15}	3.80×10^{14}	6.07×10^{14}	1.77×10^{14}

[a]Units: n = molecules/cm^3.

DOI: 10.1021/acs.jpca.5b04905
J. Phys. Chem. A XXXX, XXX, XXX−XXX

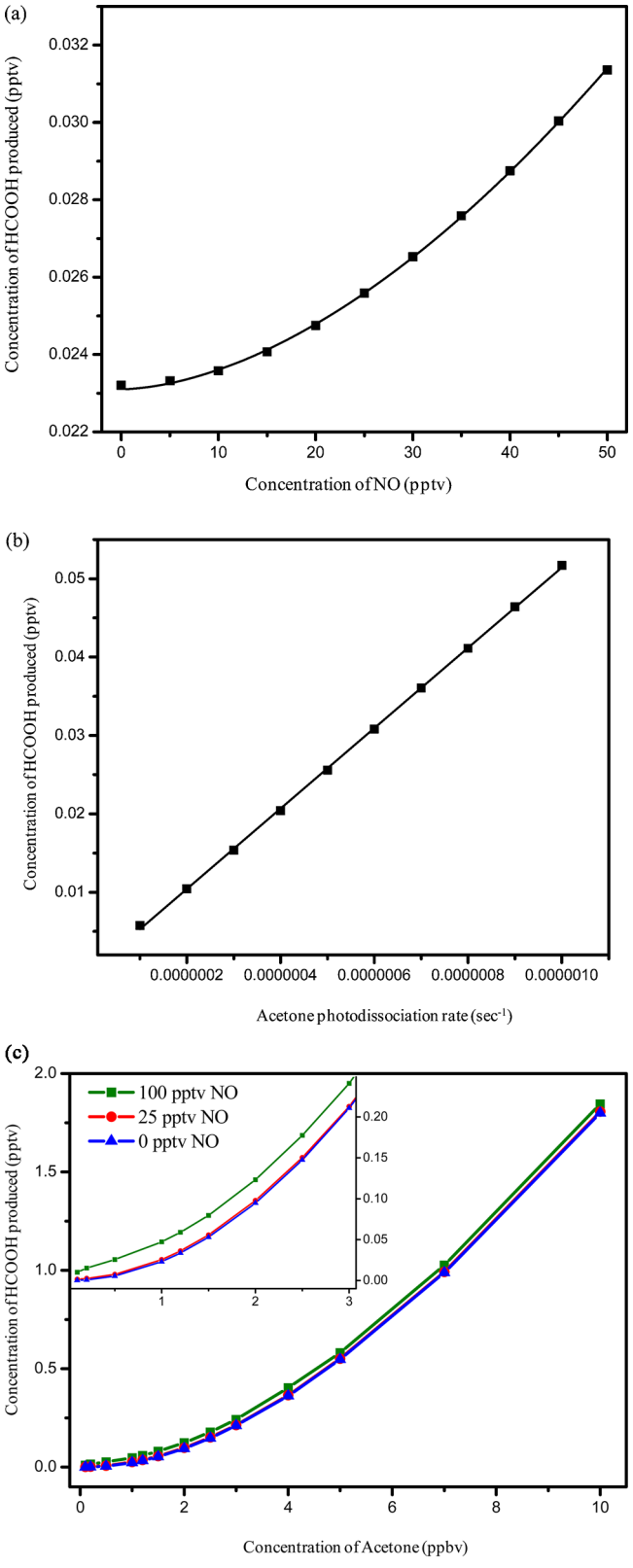

Figure 8. (a) Changes of HCOOH yields with atmospheric NO concentration as obtained from simulation. (b) Dependence of HCOOH yield on acetone photodissociation rate as obtained from simulation. (c) Change of HCOOH yield with acetone abundance for three different atmospheric concentrations of NO as obtained from simulation. The inset shows the same at a blown up scale for atmospheric acetone concentrations up to 3 ppbv.

and the reasons for such contrasting behavior are discussed below.

The atmospheric photodissociation rate also has a large effect on HCOOH production, and Figure 8b shows the dependence of acid production on the rate constant of acetone photodissociation according to our modeling study. It is seen that HCOOH production yield increases almost linearly with acetone photodissociation rate constant. To perform this simulation, the concentrations of acetone and NO are considered to be 1 ppbv and 25 pptv, respectively.

Finally, examined also in our modeling is the dependence of HCOOH production yield on atmospheric abundance of acetone, and the results are presented in Figure 8c. Three separate simulations have been performed for this purpose for three different concentrations of NO (0, 25, and 100 pptv), and in all three cases an acetone photodissociation rate of $k = 5 \times 10^{-7}$ s^{-1} has been used. It is seen that the reaction yield increases exponentially with increasing abundance of acetone for a fixed NO abundance. It is also clear that the concentration of NO has an effect on increasing HCOOH production yield, and this is more significant in the lower range of acetone concentration as shown in the inset of Figure 8c.

We now discuss the apparent unexpected behavior of atmospheric photo-oxidation as shown in Figure 8a, which indicates that HCOOH production could be increased with an increase in the atmospheric abundance of NO. The behavior is unexpected in the sense that NO is a potential quencher of peroxy radicals, the precursors of HCOOH. To understand this and also to find out the key reactions of the complex mechanism (Table 8), we adopted the following approach. Reaction modeling was performed repeatedly by omitting one of the reactions shown in Table 8 at a time, and the results are presented in Table 10.

Table 10. Effects on HCOOH Yield for Removal of a Specific Reaction at a Time in Reaction Modeling

no.	reaction omitted from simulation	HCOOH produced (pptv)	% change in HCOOH production
	original simulation	0.02559	
42	$NO + CH_3O_2 \rightarrow CH_3O + NO_2$	0.02755	7.66
43	$NO + CH_3COO_2 \rightarrow CH_3CO_2 + NO_2$	0.02676	4.57
41	$NO + HO_2 \rightarrow HO + NO_2$	0.02359	−7.82
22	$CH_3CO+O_2 \rightarrow OH + Products$	0.01049	−59.00
27	$H_2O_2 \rightarrow 2\ OH$	0.01740	−32.00
26	$OH+HCHO \rightarrow HCOOH + H$	0.00001	−99.96
44	$NO + HOCH_2O_2 \rightarrow HOCH_2O + NO_2$	0.02559	0

It is seen that if the reactions 42 and 43, i.e., reactions of NO with methyl and acetyl peroxy radicals, the precursors of HCOOH, are excluded, HCOOH yields are increased only by ∼7.7 and ∼4.6%, respectively. On the other hand, if the reaction of NO with hydroperoxy radical (reaction 41) is excluded, HCOOH production decreases by ∼7.8%, which implies that this reaction helps in HCOOH production and is responsible for the overall increase in HCOOH production with an increase in NO concentration. Reaction 41 is one of the sources of OH radical, and under atmospheric condition, it could be an important step. Two other vital sources of atmospheric OH radicals are the reaction of acetyl radical with molecular oxygen (reaction 22) and H_2O_2 dissociation (reaction 27). Exclusion of the former causes a lowering of

DOI: 10.1021/acs.jpca.5b04905
J. Phys. Chem. A XXXX, XXX, XXX−XXX

HCOOH yield by ~59%. The most vital reaction in this regard is the reaction of OH radical with formaldehyde (reaction 26), and omission of this reaction decreases the HCOOH yield by 99.96%. Thus, under atmospheric conditions, reaction of the OH radical with formaldehyde is exclusively the major source of HCOOH production in comparison to formaldehyde photo-oxidation. As a consequence, reaction 44, i.e., reaction of NO with $HOCH_2O_2$ (the intermediate for HCOOH production from formaldehyde by photo-oxidation), is insensitive on HCOOH production. However, in a reactor cell in the laboratory, we have checked via a modeling study that formaldehyde photo-oxidation is the major source of HCOOH. The reaction of OH radical with formaldehyde is a minor source of HCOOH production in the reactor cell, and its contribution is less than 1%.

Thus, from the above discussion, we infer that HCOOH production within the cell reactor of a laboratory experiment and in real atmosphere could occur via different pathways. In the atmosphere, the reaction of OH radical with formaldehyde is the dominant pathway for HCOOH formation in acetone photo-oxidation. Atmospheric abundance of acetone is a very imortant factor for HCOOH production yield. An interesting prediction of our model study is that NO assists in production of HCOOH. This is because, in the regions where NO_x concentration is as high as 1 ppbv, the model predicts that this channel can produce HCOOH in the range of ~1 pptv. Atmospheric abundance of HCOOH falls in the range of tens of pptv in the upper troposphere, whereas in the lower tropospheric region it is in the range of hundreds of pptv.[42] The amount of HCOOH production from acetone alone, as estimated here, is remarkably high, and similar estimates for other ketones having considerable atmospheric abundance could also be important.

IV. SUMMARY AND OUTLOOK

In this study, we have investigated acetone photo-oxidation in synthetic air under exposure of UV light of wavelength 311 nm. Infrared spectroscopy probing of the reaction reveals that formic acid is a major photoproduct, although there were controversies in the early days about authenticity for its formation in the same oxygen-rich environment. With an increase in the duration of light exposure, the accumulation of formic acid in the reactor cell increases linearly, and similar behavior is found also with respect to two other major photoproducts, methanol and formaldehyde. Formic acid production yield also increases with an increase in oxygen partial pressure in the reactor, but the same cause has the opposite effect on the yield of methanol. This behavior has been explained by suggesting that $HO_x^{\bullet}$ radicals, which could be produced from peroxyacetyl radical under the reaction conditions, can oxidize methanol and formaldehyde in parallel reactions. It has been stated also that in real atmosphere, because of the strong affinity of the intermediate peroxy radicals toward NO_x, the yield of formic acid production could be seriously impaired. As laboratory verification of this possibility, yields of formic acid formation were measured in the presence of nitric oxide of similar atmospheric relative abundances with respect to acetone. However, the measured data show that the effect is quite insignificant, and similar behavior is also suggested by the reaction-modeling study. Furthermore, to understand the implications of these laboratory findings on the actual chemistry of our atmosphere, reaction modeling has been performed with the realistic atmospheric abundances of acetone and nitic oxide. The results show that NO_x in the atmosphere enhances formic acid formation. The study also reveals that, in the atmosphere, formaldehyde oxidation to formic acid by OH radical is a more preferred oxidation channel compared to photo-oxidation. It is expected that the findings presented here could have a broader implication on the issue of the missing sources of formic acid in the earth's atmosphere.

■ ASSOCIATED CONTENT

Supporting Information

Table depicting the variation of quantum yields with variation of surface to volume ratio of the reaction cell. The Supporting Information is available free of charge on the ACS Publications website at DOI: 10.1021/acs.jpca.5b04905.

■ AUTHOR INFORMATION

Corresponding Authors

*E-mail: pcac@iacs.res.in. Tel: +91 33 2473 4971 (ext 1470). Fax: +91 33 2473 2805.

*E-mail: pctc@iacs.res.in. Tel: +91 33 2473 4971 (ext 1470). Fax: +91 33 2473 2805.

Notes

The authors declare no competing financial interest.

■ ACKNOWLEDGMENTS

We sincerely acknowledge the valuable discussions and helpful guidelines received from Prof. A. R. Ravishankara of Colorado State University to complete the work described in this paper. The financial support received from the Department of Science and Technology, Government of India, under Scheme No. SB/S1/PC-027/2013 is acknowledged. A.C. thanks CSIR, Government of India, for a Senior Research Fellowship, and P.C. thanks DST INSPIRE Scheme for a Junior Research Fellowship.

■ REFERENCES

(1) Paulot, F.; Wunch, D.; Crounse, J. D.; Toon, G. C.; Millet, D. B.; DeCarlo, P. F.; Vigouroux, C.; Deutscher, N. M.; González Abad, G.; Notholt, J.; et al. Importance of Secondary Sources in the Atmospheric Budgets of Formic and Acetic Acids. *Atmos. Chem. Phys.* **2011**, *11*, 1989−2013.

(2) Stavrakou, T.; Müller, J.-F.; Peeters, J.; Razavi, A.; Clarisse, L.; Clerbaux, C.; Coheur, P.-F.; Hurtmans, D.; De Maziere, M.; Vigouroux, C.; et al. Satellite Evidence for a Large Source of Formic Acid from Boreal and Tropical Forests. *Nat. Geosci.* **2012**, *5*, 26−30.

(3) Millet, D. B. Natural Atmospheric Acidity. *Nat. Geosci.* **2012**, *5*, 8−9.

(4) Sing, H. B.; Kanakidou, M.; Crutjen, P. J.; Jacob, D. J. High Concentrations and Photochemical Fate of Oxygenated Hydrocarbons in the Global Troposphere. *Nature* **1995**, *378*, 50−54.

(5) Fischer, E. V.; Jacob, D. J.; Millet, D. B.; Yantosca, R. M.; Mao, J. The Role of Ocean in the Global Atmospheric Budget of Acetone. *Geophys. Res. Lett.* **2012**, *39*, L01807 (1−5).

(6) Jacob, D. J.; Field, B. D.; Jin, E. M.; Bey, I.; Li, Q.; Logan, J. A.; Yantosca, R. M.; Singh, H. B. Atmospheric Budget of Acetone. *J. Geophys. Res.* **2002**, *107*, ACH 5 (1−17).

(7) Osborne, A. D.; Pitts, J. N.; Fowler, S. L. Investigation of the Photooxidation of Acetone at 3130 Å Using Infrared Analysis. *J. Phys. Chem.* **1961**, *65*, 1622−1625.

(8) Pearson, G. S. The Photooxidation of Acetone. *J. Phys. Chem.* **1963**, *67*, 1686−1692.

(9) Hoare, D. E.; Whytock, D. A. Photooxidation of Acetone Vapour. *Can. J. Chem.* **1967**, *45*, 865−872.

(10) Cohen, A. Methyl Hydroperoxyde in Photooxidation of Acetone. *J. Chem. Phys.* **1967**, *47*, 3828−3831.

DOI: 10.1021/acs.jpca.5b04905
J. Phys. Chem. A XXXX, XXX, XXX−XXX

(11) Gardner, E. P.; Wijayaratne, R. D.; Calvert, J. G. Primary Quantum Yields of Photodecomposition of Acetone in Air under Tropospheric Conditions. *J. Phys. Chem.* **1984**, *88*, 5069−5076.
(12) McKeen, S. A.; Gierczak, T.; Burkholder, J. B.; Wennberg, P. O.; Hanisco, T. F.; Keim, E. R.; Gao, R.-S.; Liu, S. C.; Ravishankara, A. R.; Fahey, D. W. The Photochemistry of Acetone in the Upper Troposphere: A Source of Odd Hydrogen Radicals. *Geophy. Res. Lett.* **1997**, *24*, 3177−3180.
(13) Gierczak, T.; Burkholder, J. B.; Bauerle, S.; Ravishankara, A. Photochemistry of Acetone under Tropospheric Conditions. *Chem. Phys.* **1998**, *231*, 229−244.
(14) Emrich, M.; Warneck, P. Photodissociation of Acetone in Air: Dependence on Pressure and Wavelength. Behavior of the Excited Singlet State. *J. Phys. Chem. A* **2000**, *104*, 9436−9442.
(15) Aloisio, S.; Francisco, J. S. The Photochemistry of Acetone in the Presence of Water. *Chem. Phys. Lett.* **2000**, *329*, 179−184.
(16) Blitz, M. A.; Heard, D. E.; Pilling, M. J. OH Formation from $CH_3CO + O_2$: A Convenient Experimental Marker for Acetyl Radical. *Chem. Phys. Lett.* **2002**, *365*, 374−379.
(17) Suryaraman, M. G.; Viswanatha, A. Preparation of Nitric Oxide: Some Laboratory Methods. *J. Chem. Educ.* **1949**, *26*, 594−596.
(18) Sharpe, S. W.; Johnson, T. J.; Sams, R. L.; Chu, P. M.; Rhoderick, G. C.; Johnson, P. A. Gas-Phase Databases for Quantitative Infrared Spectroscopy. *Appl. Spectrosc.* **2004**, *58*, 1452−1461.
(19) Herr, D. S.; Noyes, W. A. Photochemical Studies. XXXI. A Systematic Study of the Near Ultraviolet Photochemical Decomposition of Acetone. *J. Am. Chem. Soc.* **1940**, *62*, 2052−2059.
(20) Braun, W.; Herron, J. T.; Kahaner, D. K. Acuchem: A Computer Program for Modeling Complex Chemical Reaction Systems. *Int. J. Chem. Kinet.* **1988**, *20*, 51−62.
(21) Dawson, M. L.; Varner, M. E.; Perraud, V.; Ezell, M. J.; Gerber, R. B.; Finlayson-Pitts, B. J. Simplified Mechanism for New Particle Formation from Methanesulfonic Acid, Amines, and Water via Experiments and Ab Initio Calculations. *Proc. Natl. Acad. Sci. U. S. A.* **2012**, *109*, 18719−18724.
(22) Copeland, G.; Ghosh, M. V.; Shallcross, D. E.; Percival, C. J.; Dyke, J. M. A Study of the Ethene-Ozone Reaction with Photoelectron Spectroscopy: Measurement of Product Branching Ratios and Atmospheric Implications. *Phys. Chem. Chem. Phys.* **2011**, *13*, 14839−14847.
(23) Orlando, J. J.; Tyndall, G. S. The Atmospheric Oxidationof Ethyl Formate and Ethyl Acetate over a Range of Temperatures and Oxygen Partial Pressures. *Int. J. Chem. Kinet.* **2010**, *42*, 397−413.
(24) Orlando, J. J. The Atmospheric Oxidation of Diethyl Ether: Chemistry of the $C_2H_5−O−CH(O)CH_3$ Radical between 218 and 335 K. *Phys. Chem. Chem. Phys.* **2007**, *9*, 4189−4199.
(25) DeMore, W. B.; Sander, S. P.; Golden, D. M.; Hampson, R. F.; Kurylo, M. J.; Howard, C. J.; Ravishankara, A. R.; Kolb, C. E.; Molina, M. J. *Chemical Kinetics and Photochemical Data for Use in Stratospheric Modeling*; JPL Pub. No. 97-4; Jet Propulsion Laboratory: Pasadena, 1997.
(26) Tyndall, G. S.; Orlando, J. J.; Wallington, T. J.; Hurley, M. D. Pressure Dependence of the Rate Coefficients and Product Yields for the Reaction of CH_3CO Radicals with O_2. *Int. J. Chem. Kinet.* **1997**, *29*, 655−663.
(27) Atkinson, R.; Baulch, D. L.; Cox, R. A.; Crowley, J. N.; Hampson, R. F.; Hynes, R. G.; Jenkin, M. E.; Rossi, M. J.; Troe, J. Evaluated Kinetic and Photochemical Data for Atmospheric Chemistry: Volume II - Gas Phase Reactions of Organic Species. *Atmos. Chem. Phys.* **2006**, *6*, 3625−4055.
(28) Maricq, M. M.; Szente, J. J. The $CH_3C(O)O_2$ Radical. Its UV Spectrum, Self-Reaction Kinetics, and Reaction with CH_3O_2. *J. Phys. Chem.* **1996**, *100*, 4507−4513.
(29) Lightfoot, P. D.; Cox, R. A.; Crowley, J. N.; Destriau, M.; Hayman, G. D.; Jenkin, M. E.; Moortgat, G. K.; Zabel, F. Organic peroxy radicals: Kinetics, spectroscopy and tropospheric chemistry. *Atmos. Environ., Part A* **1992**, *26*, 1805−1961.
(30) Atkinson, R.; Baulch, D. L.; Cox, R. A.; Hampson, R. F.; Kerr, J. A.; Troe, J. Evaluated Kinetic and Photochemical Data for Atmospheric Chemistry Supplement IV, IUPAC Subcommittee on Gas Kinetic Data Evaluation for Atmospheric Chemistry. *J. Phys. Chem. Ref. Data* **1992**, *21*, 1125−1568.
(31) Roehl, C. M.; Bauer, D.; Moortgat, G. K. Absorption Spectrum and Kinetics of the Acetylperoxy Radical. *J. Phys. Chem.* **1996**, *100*, 4038−4047.
(32) Atkinson, R.; Baulch, D. L.; Cox, R. A.; Hampson, R. F., Jr; Kerr, J. A.; Rossi, M. J.; Troe, J. Evaluated Kinetic, Photochemical and Heterogenious Data for Atmospheric Chemistry Supplement V, IUPAC Subcommittee on Gas Kinetic Data Evaluation for Atmospheric Chemistry. *J. Phys. Chem. Ref. Data* **1997**, *26*, 521−1011.
(33) Veyret, B.; Rayez, J. C.; Lesclaux, R. Mechanism of the Photooxidation of Formaldehyde Studied by Flash Photolysis of CH_2O-O_2-NO Mixtures. *J. Phys. Chem.* **1982**, *86*, 3424−3430.
(34) Yetter, R. A.; Rabitz, H.; Dryer, F. L.; Maki, R. G.; Klemm, R. B. Evaluation of the Rate Constant for the Reaction $OH+H_2CO$: Application of Modeling and Sensitivity Analysis Techniques for Determination of the Product Branching Ratio. *J. Chem. Phys.* **1989**, *91*, 4088−4097.
(35) Rhee, T. S.; Brenninkmeijer, C. A. M.; Röckmann, T. Hydrogen Isotope Fractionation in the Photolysis of Formaldehyde. *Atmos. Chem. Phys.* **2008**, *8*, 1353−1366.
(36) Lightfoot, P. D.; Veyret, B.; Lesclaux, R. Flash Photolysis Study of the $CH_3O_2 + HO_2$ Reaction 248 and 573 K. *J. Phys. Chem.* **1990**, *94*, 708−714.
(37) Kan, C. S.; Calvert, J. G.; Shaw, J. H. Reactive Channels of the CH_3O_2-CH_3O_2 Reaction. *J. Phys. Chem.* **1980**, *84*, 3411−3417.
(38) Sander, S. P.; Abbatt, J.; Barker, J. R.; Burkholder, J. B.; Friedl, R. R.; Golden, D. M.; Huie, R. E.; Kolb, C. E.; Kurylo, M. J.; Moortgat, G. K. et al. *Chemical Kinetics and Photochemical Data for Use in Atmospheric Studies*; Evaluation No. 17, JPL Publication 10-6; Jet Propulsion Laboratory: Pasadena, 2011; http://jpldataeval.jpl.nasa.gov.
(39) Atkinson, R.; Baulch, D. L.; Cox, R. A.; Crowley, J. N.; Hampson, R. F.; Hynes, R. G.; Jenkin, M. E.; Rossi, M. J.; Troe, J. Evaluated Kinetic and Photochemical Data for Atmospheric Chemistry: Volume I − Gas Phase Reactions of Ox, HOx, NOx and SOx Species. *Atmos. Chem. Phys.* **2004**, *4*, 1461−1738.
(40) Baggott, J. E.; Frey, H. M.; Lightfoot, P. D.; Walsh, R. The Absorption Cross Section of HCO Radical at 614.59 nm and the Rate Constant for $HCO+HCO \rightarrow H_2CO+CO$. *Chem. Phys. Lett.* **1986**, *132*, 225−230.
(41) Jacob, D. J. *Introduction to Atmospheric Chemistry*; Princeton University Press: Princeton, 1999.
(42) González Abad, G. G.; Bernath, P. F.; Boone, C. D.; McLeod, S. D.; Manney, G. L.; Toon, G. C. Global Distribution of Upper Tropospheric Formic Acid from the ACE-FTS. *Atmos. Chem. Phys.* **2009**, *9*, 8039−8047.

DOI: 10.1021/acs.jpca.5b04905
J. Phys. Chem. A XXXX, XXX, XXX−XXX